

Acquisition time optimization of positron emission tomography studies by use of a regression function derived from torso cross-sections and noise-equivalent counts

Yoshiharu Kangai^{1,2} · Hideo Onishi¹

Received: 14 October 2015 / Revised: 10 January 2016 / Accepted: 12 January 2016 / Published online: 21 January 2016
© Japanese Society of Radiological Technology and Japan Society of Medical Physics 2016

Abstract In this study, we aimed to optimize the positron emission tomography (PET) acquisition time for individual patients by employing a regression function derived from torso cross-sections by using computed tomography (CT) attenuation corrections and the noise-equivalent counts (NECs). We initially determined the standard image quality or the standard NEC at our institution by visually assessing the images acquired from 61 patients. We measured the NECs of the livers and the torso cross-sections of 165 patients who were evaluated with PET/CT with ¹⁸F-2-fluoro-2-deoxy-D-glucose on the basis of our standard protocol of 120 s/bed position. The optimal acquisition time (OPT) was calculated as the product of the ratio of the standard NEC to the estimated NEC multiplied by 120 s. The estimated NEC was derived from the oval cross-section of each patient by use of the regression function. We evaluated the validity of the OPT equation in 59 additional patients. We determined 5.83 Mcounts as the standard NEC at our institution. The mean OPTs in a group of 59 patients of whom 20, 19, and 20 were underweight, normal-weight, and overweight, respectively, were 106.3 ± 18.0 , 137.1 ± 4.6 , and 172.1 ± 24.3 s, respectively. After optimization, the NECs for normal-weight and overweight patients increased by 14 and 43 %, respectively, compared with the NECs attained with use of the

conventional acquisition time (120 s). Using the regression function based on the torso cross-sections and the NECs enabled optimizations of the PET acquisition times for individual patients.

Keywords Image acquisition · Obesity · Radioactivity · Diagnosis · ¹⁸F-fluorodeoxyglucose positron emission tomography · Computed tomography

1 Introduction

Positron emission tomography (PET) imaging with ¹⁸F-2-fluoro-2-deoxy-D-glucose (¹⁸F-FDG) is widely used in clinical oncology for facilitating the diagnosis of a wide variety of cancers [1–3]. In general, the amount of ¹⁸F-FDG that is injected into a patient varies according to their physical constitution if it is produced in-house. On the other hand, the commercially produced ¹⁸F-FDG that is manufactured in radiopharmaceutical facilities in Japan is dispensed after calibration at a 185 MBq vial per patient, and then it is delivered to more than 50 % of the PET facilities in Japan. However, the upper limit of the available dose is 350 MBq per patient, because commercial ¹⁸F-FDG is delivered about 100 min after it is calibrated.

The quality of clinical ¹⁸F-FDG PET images from overweight patients is often poor [4, 5], and this can be improved [6–9] by increasing the radiation dose administered or by extending the acquisition time. Lartizien et al. [7] reported that the maximum noise-equivalent count (NEC) rate in the three-dimensional (3D) mode is well defined, and that the corresponding injected dose depends on a patient's height and weight. On the other hand, Masuda et al. [8] suggested that the quality of the images acquired from heavier patients could be maintained by

✉ Yoshiharu Kangai
kangai@med.kawasaki-m.ac.jp

¹ Program in Biological System Sciences, Graduate on School of Comprehensive Scientific Research, Prefectural University of Hiroshima, 1-1 Gakuenmachi, Mihara, Hiroshima 723-0053, Japan

² Department of Radiology, Kawasaki Medical School Hospital, 577 Matsushima, Kurashiki, Okayama 701-0192, Japan

scanning for longer periods, because increasing the dose of radiation per patient kilogram did not improve the quality of lutetium oxyorthosilicate PET/computed tomography (CT) images. The uniform dose of 185 MBq in the commercially ^{18}F -FDG causes difficulties for overweight patients when attempts are made to increase the injected dose in accordance with a patient's weight [10]. Therefore, image quality is controllable only by optimizing of the acquisition time.

The NEC is often used for assessment of the quality of patients' PET images. Mizuta et al. [11] reported that the NEC density (NECD) is computed as the NEC patient (NECP) divided by the average cross-sectional area of the subject's body that is obtained from the transmission images. The NECP is the number of NEC per axial length unit. Therefore, the NECD, or the NEC count per unit volume, may be a useful indicator of image quality in clinical trials. However, the calculation of the unit volumes from transmission images is complex. Most PET systems are combined with CT [12, 13]; therefore, we considered the possibility of using a correction based on the cross-sectional areas obtained from CT images and the NECs because measuring the cross-sectional area from a CT image is easier and faster than calculating the unit volume. In a previous study, the quality of PET images was assessed, while patients held both arms up, with use of bodyweight and the body mass index (BMI). Shimada et al. [14] reported that the quality of the PET images produced when the patients had both arms down was clearly inferior compared with those obtained when the patients held their arms up. However, a PET/CT study of images obtained when patients held their arms up, revealed cold artifacts associated with arm motion on the PET images [15]. Furthermore, it is difficult for elderly patients to hold up their arms for prolonged periods; therefore, we utilized a cross-section that includes both arms and reflects a patient's habits when they have their arms down.

In this study, we aimed to optimize the PET acquisition time for individual patients by applying a regression function obtained by simply calculating the cross-sections from CT images and the NECs that will enable PET images of a constant quality to be attained by facilities that use commercially produced ^{18}F -FDG.

2 Materials and methods

2.1 Study design

This study comprised three parts. We initially defined the standard quality, or standard NEC, for PET images that is required for achievement of accurate diagnoses at our institution (group 1: $n = 61$). The standard NEC was

determined from its relationship with the NEC and from visual assessments. We constructed an equation to determine the optimal acquisition time (OPT) from a regression analysis of the relationship between the NEC and the patients' oval cross-sections (OCSs) (group 2: $n = 165$). We then assessed the validity of the OPTs by applying the regression function to the patients from group 3 ($n = 59$). Furthermore, we compared the NECs attained by use of the conventional acquisition time of 120 s with those obtained by use of the OPTs from the patients in group 3. The patient groups did not overlap.

2.2 Positron emission tomography/computed tomography system

We assessed the patients by using a Discovery STE PET/CT system (GE Healthcare, Waukesha, WI, USA), which comprised an 8-multislice CT scanner and a PET scanner that used $\text{Bi}_4\text{Ge}_3\text{O}_{12}$ as the detector material. The transaxial field of view (FOV) in the PET system was 700 mm, the axial FOV was 157 mm, and the system generated 47 planes with a slice thickness of 3.37 mm per bed position. The energy window was set between 425 and 650 keV in 3D mode, and the coincident timing window was 9.6 ns. The spatial resolution of the 3D mode at full-width at half-maximum (FWHM) was 5.12 mm at a 1 cm offset from the center, and the radial and tangential resolutions were 5.89 and 5.47 mm, respectively, at a 10 cm offset from the center [16]. The images were analyzed on a Xeleris workstation (GE Healthcare).

2.3 Patients and imaging protocol

Kawasaki Medical School and Kawasaki Medical School Hospital's institutional review board approved this retrospective study (protocol no. 1990), and it provided an exemption for reviewing the PET/CT data from 285 patients (134 women and 151 men) with a mean age of 61.4 ± 12.7 years and a mean weight of 59.7 ± 13.1 kg. We excluded patients who had liver metastases or hyperglycemia before the ^{18}F -FDG was injected. All of the patients were placed in the supine position on the imaging table with their arms down. Whole-body images were acquired in list mode in 8 bed positions, from the vertex to the upper or middle thigh, for 120–240 s per bed position. Scanning began 60 min after the ^{18}F -FDG injection in groups 1 and 2. We acquired the PET images from the patients in group 3 by using the OPT in list mode, although the minimum acquisition time was set at 120 s.

Changing the injected dose in accordance with the physical constitution of each patient was difficult. The mean level of radioactivity in the injected ^{18}F -FDG was 242.5 ± 31.2 MBq (range = 173.2–305.2 MBq). The

overlap between the bed positions was set at 11 planes, corresponding to 26.7 mm, which is the default value for 3D acquisitions. The PET images were reconstructed by use of CT-based attenuation corrections, a scatter correction algorithm (i.e., a model-based scatter correction [15, 17]), and 3D-ordered subset expectation maximization by use of VUE Point PlusTM (GE Healthcare), 2 iterations, and 20 subsets. A post-reconstruction Gaussian filter with a spatial resolution of 5.14 mm at full-width at half-maximum (FWHM) was applied.

2.4 Visual scoring and determination of the standard noise-equivalent count

Sixty-one patients formed group 1, which included 28 women and 33 men. The group's mean weight was 60.9 ± 12.7 kg, and the mean dose of radiation administered was 232.8 ± 30.9 MBq. The list-mode datasets were trimmed for 120 s and reconstructed. Four independent reviewers, including 1 specialist in nuclear medicine physician, 2 nuclear medicine technologists, and 1 radiological technologist, who were experienced in evaluating clinical ¹⁸F-FDG PET images, visually assessed the uniformity of the transverse and coronal liver slices of the largest liver sections and the maximum intensity projection images [11]. All of the reviewers were blinded to the patients' information. The quality of all of the PET images was scored from 1 to 5, corresponding to non-diagnostic, poor, moderate, good, or excellent, respectively, on the basis of the visual assessments [11, 18]. Specialist in nuclear medicine physician has made sufficient training for all reviewers before visual scoring test. The visual scores were averaged, and their relationships with the NECs are determined from Eq. 1, which was developed by Fukukita et al. [19], as follows:

$$\text{NEC} = (1 - sf)^2 \frac{(P - R)}{(P - R) + (1 + k)R}, \quad (1)$$

where P , R , and sf are the prompts, randoms, and scatter fraction, respectively. The NECs for the bed positions that included the liver were calculated for each patient. The factor k differs according to the method used for correcting the random coincidences. We evaluated the random events by using a delayed event subtraction window; therefore, k was set to 1. In Eq. 1, P , R , and sf were obtained from the patient's raw data; these can be extracted directly from the recorded file header on GE Discovery STE PET/CT scanners [20, 21]. The relationship between the average visual score and the NEC was evaluated, and the standard NEC used at our institution was determined from the visual score. The standard NEC at our institution was defined as an average visual score of 3 points (moderate).

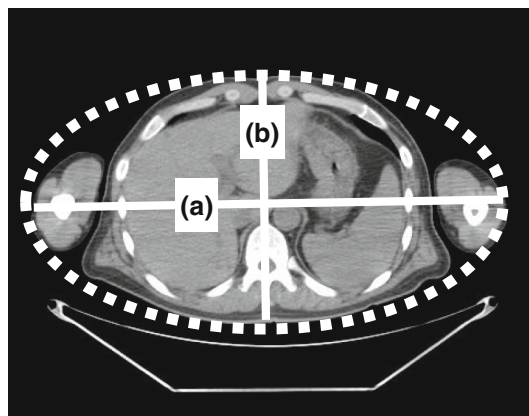


Fig. 1 Measurements of torso cross-section on transverse computed tomography images. The oval cross-section was calculated from the major axis (a) and the minor axis (b) a Xeleris workstation

2.5 Adequacy of the oval cross-section

We assumed that the torso cross-sections of all of the patients were oval and easily measured. We retrospectively measured the cross-sectional areas and the OCSs of the liver in the CT images from 61 patients (group 1). The cross-section was measured by extraction of an outline of the torso on a transaxial image by use of Xeleris software. The OCSs were calculated from the major and minor axes (Fig. 1) from Eq. 2, as follows:

$$\text{OCS}(\text{mm})^2 = \pi \times \frac{\text{major axis}(\text{mm})}{2} \times \frac{\text{minor axis}(\text{mm})}{2}, \quad (2)$$

where π is the circular constant (3.14). We determined the relationships between the torso cross-sections and the OCSs in all of the patients by using the liver sections among the transverse CT images, and we then determined the correlation between the measured cross-section and the OCS for each patient.

2.6 Estimation of the noise-equivalent count from the regression function

The regression function was generated from the relationship between the NEC and weight, BMI, and OCS in group 2 ($n = 165$), which comprised 81 women and 84 men; who had a mean weight and BMI of 59.5 ± 12.8 kg and 22.9 ± 3.6 kg/m², respectively. The mean dose of radiation administered was 244.2 ± 31.5 MBq. The PET images were obtained with an acquisition time of 120 s/bed position. In generally, the uptake of FDG is related to weight and BMI [4–10], but alternative patient-dependent parameters may be more appropriate. Therefore, the NEC was displayed as a function of various patient-dependent

parameters and fitted in a power function. The coefficient of determination (R^2) was applied for evaluation of an optimal parameter. The estimated NEC (ENEC) was determined from the regression function by measurement of the OCS as described previously.

2.7 Optimal acquisition time and NEC

The quality of the PET images was improved by prolonging of the acquisition time. The NEC of obese patients is low, and the quality of the images acquired from these patients can be maintained by scanning for longer periods [4, 8, 9]. We assumed that the OPT could be calculated as the product of the conventional acquisition time (120 s) multiplied by the NEC/ENEC ratio, which was determined from the OCS, for the individual patients from Eq. 3, as follows:

$$\text{OPT} (s) = 120 (s) \times \frac{\text{Standard NEC (Mcount)}}{\text{ENEC (Mcount)}}. \quad (3)$$

We assessed the validity of the calculated OPT in the patients from group 3 ($n = 59$), which comprised 25 women and 34 men, who had a mean weight of 59.8 ± 14.9 kg. The mean dose of radiation administered was 235.7 ± 32.4 MBq. Group 3 was further categorized into small, normal, and overweight OCS subgroups (Table 1), and the average OPTs and optimized NECs were calculated for each subgroup. Subsequently, we compared the NECs attained by using the conventional acquisition time of 120 s with those obtained by using the OPTs from the patients in group 3. Furthermore, the relationship with the optimized NEC that used the OPT and OCS was evaluated in group 3.

2.8 Statistical analysis

The data were statistically analyzed by use of Statcel 3-The Useful Add-in Forms on Excel—3rd ed. (OMS Publishing Inc, Tokorozawa, Saitama, Japan). The correlations between the visual scores and the NECs were determined by use of Spearman's visual score and, probability values of <0.05 were considered to indicate significance. The

correlation between the measured cross-sectional area and the OCS was determined for each patient by use of Pearson's correlation coefficient, and p values of <0.05 were considered statistical significant.

3 Results

3.1 Visual scoring and determination of the standard noise-equivalent count

Figure 2 shows the NEC as a function of the average visual scores for 61 patients. The visual scores were correlated significantly with the NEC. The gradient of the regression function was $y = 0.705x - 1.11$ ($r = 0.79$, $p < 0.001$). When a moderate visual score of 3.0 was substituted for y , the NEC (x) was 5.83 Mcounts, as determined from the regression function. Therefore, 5.83 Mcounts were used as the standard NEC at our institution.

3.2 Adequacy of the oval cross-section

Figure 3 shows a scatter plot of the OCSs of the torsos compared with the measured cross-sectional areas and the closely fitted line ($r = 0.97$, $p < 0.001$). The regression function was $y = 1.05x + 60.7$.

3.3 Estimation of the noise-equivalent count from the regression function

Figure 4a–c shows the coefficient of determination of NECs as a function of the weight, BMI, and OCS, which were calculated as 0.6096, 0.5684, and 0.7178, respectively. The good correlation is those where the OCS is used as the patient-dependent parameters. We used the OCS in the analysis because this will be the most accurate to implement, and the coefficient of determination was at near 1.0.

Figure 4c shows the regression functions determined from group 2 ($n = 165$) by use of a power function approximation, as follows:

$$\text{ENEC} = 4472.7 \times \text{OCS}^{-1.014}. \quad (4)$$

Table 1 Patient subgroup data

Subgroup category	Number of patients	Oval cross-section (cm ²)	Weight (kg)	BMI (kg/m ²)	Injected activity (MBq)	Scatter fraction factor
Underweight	20	619.8 ± 103.6	46.7 ± 7.5	19.7 ± 2.5	232.8 ± 30.9	0.347 ± 0.035
Normal-weight	19	796.8 ± 26.6	60.2 ± 6.0	22.1 ± 4.7	244.2 ± 31.5	0.366 ± 0.027
Overweight	20	997.2 ± 139	76.7 ± 12.1	28.1 ± 0.9	235.7 ± 32.4	0.409 ± 0.026

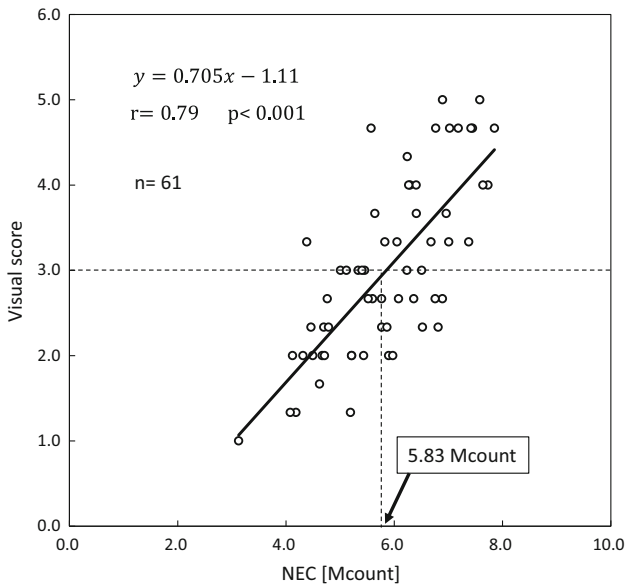


Fig. 2 The noise-equivalent counts (NECs) versus the average visual scores in whole-body ¹⁸F-2-fluoro-2-deoxy-D-glucose images acquired with use of a discovery STE positron emission tomography/computed tomography scanner. The *dotted lines* indicate the moderate visual scores of three points and the standard NEC of 5.83 Mcounts. NEC, noise-equivalent count

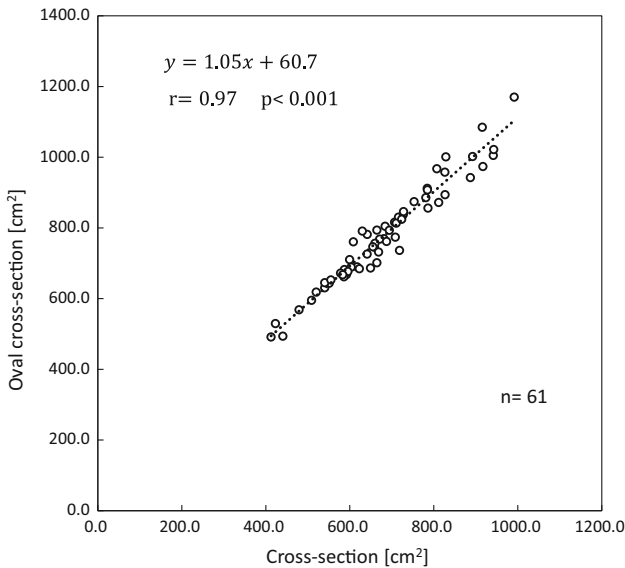


Fig. 3 Linear regression of the oval cross-sections as a function of the torso cross-sections derived from 61 patients

3.4 Optimal acquisition time and NEC

We created a formula with which to calculate the OPT after expanding the resulting regression function, as follows:

$$OPT = 120 \times \frac{5.83}{4472.7 \times OCS^{-1.014}} \quad (5)$$

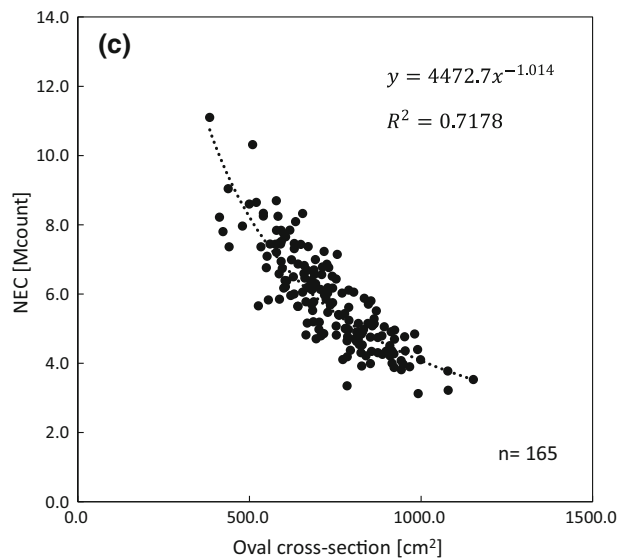
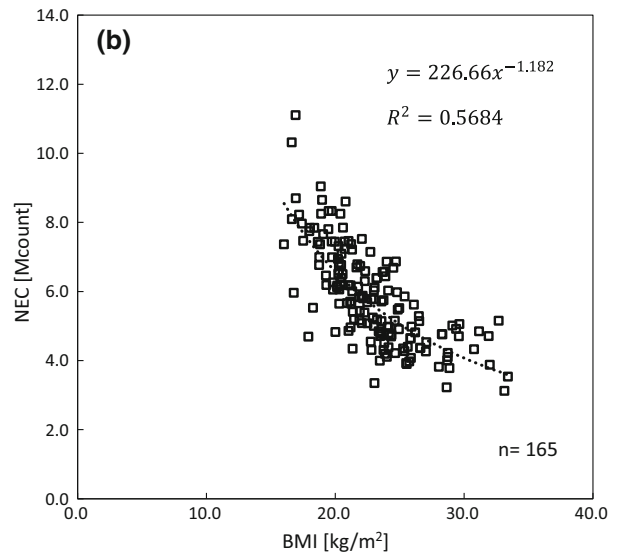
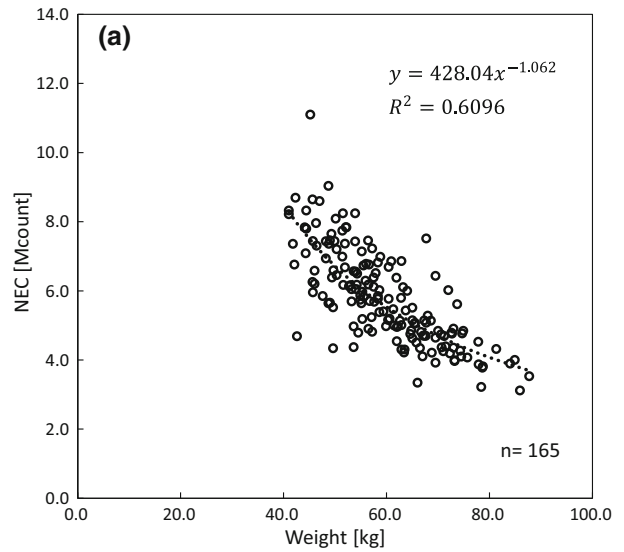


Fig. 4 Noise-equivalent counts as a function of the weight **a**, body mass index **b**, and oval cross-sections **c** derived from 165 patients. The positron emission tomography images were acquired for 120 s per bed position. *NEC* noise-equivalent count

Figure 5 shows the relationship between the NECs attained by use of the conventional acquisition time of 120 s and those obtained by use of the OPTs for each OCS subgroup. Compared with the conventional acquisition time of 120 s, the mean acquisition time was 13.7 s shorter for the underweight patients and 17.1 and 52.1 s longer for the normal-weight and overweight patients, respectively. The average optimized NECs for the underweight, normal-weight, and overweight patients were 5.49, 6.26, and 5.34 Mcounts, respectively. The NEC between 120 s and the OPT decreased by an average of 1.95 Mcounts (−26.2 %) in the underweight patients. The optimized NECs for the normal-weight and overweight patients increased by an average of 0.77 Mcounts (14.0 %) and 1.55 Mcounts (43 %), respectively, compared with those obtained at the conventional acquisition time of 120 s. The optimized NEC for patients with large OCSs had a tendency to fall below the standard NEC of 5.83 Mcounts (Fig. 6). However, the optimized NECs had an almost constant value.

Figure 7 shows the axial and coronal PET images that were acquired from three patients for 120 s, and it shows a comparison of these images with those obtained after adjustment of the acquisition times. The uniformity of the liver images from an overweight patient (bottom column) improved when Eq. 5 was applied. The quality of the optimized PET images improved in normal-weight and

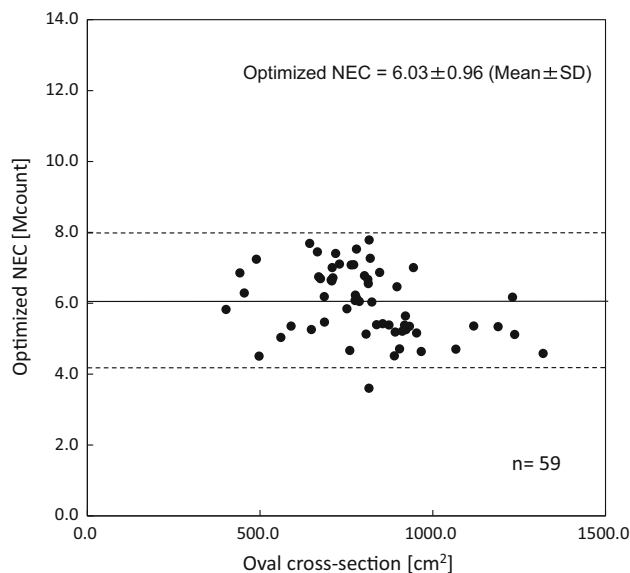


Fig. 6 Scatter plot of the optimized noise-equivalent counts against the oval cross-section values in 59 patients. The *middle horizontal line* represents the mean value of optimized NECs. The *upper and lower dotted lines* represent the 95 % confidence interval limits. *NEC* noise-equivalent count

overweight patients, but it remained the same in underweight patients.

4 Discussion

A considerable amount of effort over several years has been directed toward optimizing ¹⁸F-FDG PET/CT acquisition protocols in many institutions [22–24]. The quality

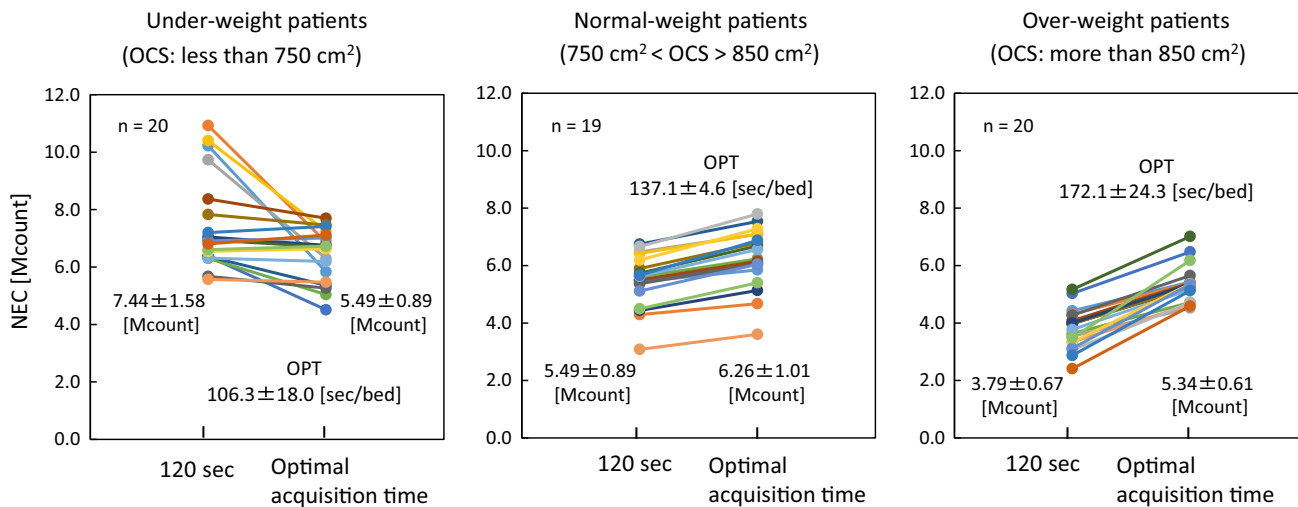


Fig. 5 Comparison of the noise-equivalent counts obtained at the conventional acquisition time of 120 s with the optimal acquisition times in the liver for each subgroup. The mean optimal acquisition times were 106.3 ± 18.0, 137.1 ± 6.5, and 172.1 ± 24.3 s, and the

oval cross-section values were less than 750 cm², 750–850 cm², and more than 850 cm² for the underweight, normal-weight, and overweight patients, respectively. *NEC* noise-equivalent count

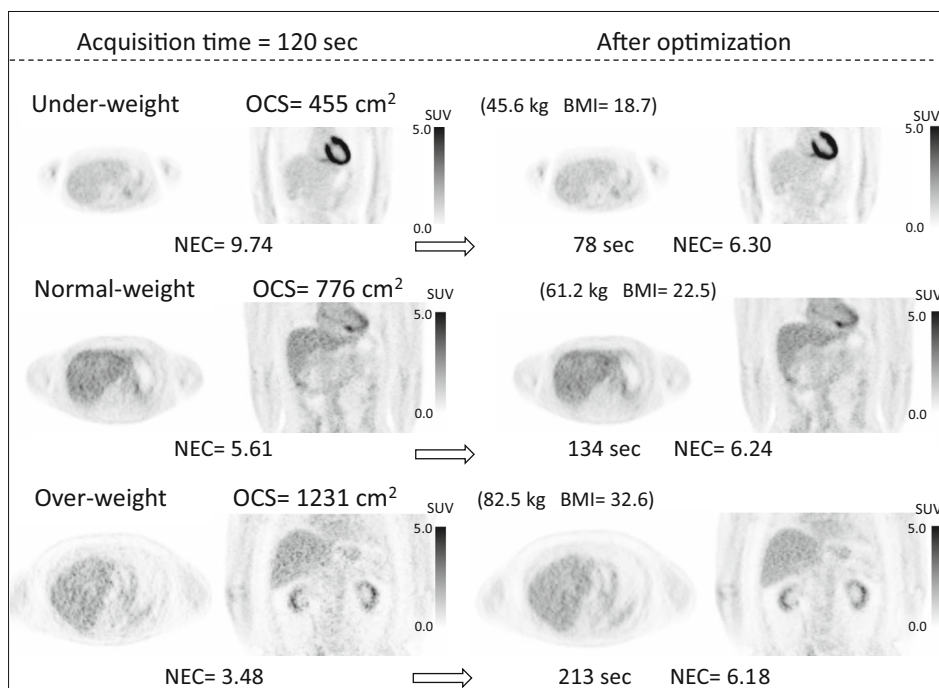


Fig. 7 Comparison of the transaxial and coronal positron emission tomography images attained at conventional (120 s) and optimal acquisition times. The standardized uptake value in each image is scaled from 5.0 to 0.0. Image quality after 120 s of acquisition (*left*) is

comparable to that after optimization (*right*) for the lighter patient (*top column*) and had clearly improved for normal-weight (*middle column*) and overweight (*bottom column*) patients. *BMI* body mass index, *NEC* noise-equivalent count, *OCS* oval cross-section

of PET images depends on the dose of radiation and on the physical constitution of the patient [4, 7]. Therefore, the NEC is correlated significantly with image quality, and it often serves as an index of image quality [11, 23]. We have optimized the amount of time required for acquiring uniform PET images from cross-sections of the torso on CT images in clinical studies. We have measured the NECs in the bed positions that included the liver in all of the patients. We selected these bed positions because the liver is the largest organ that has a relatively uniform and constant radiotracer uptake [8].

The NECs were closely correlated with the visual scores, indicating that increasing the NEC significantly improved PET image quality. This finding concurs with those reported by Masuda et al. [8], Nagaki et al. [10], and McDermott et al. [18]. We determined a standard NEC of 5.83 Mcounts from the linear regression functions and considered that our method of calculating a standard NEC by using the visual scores was suitable for improving image quality. The torso cross-sections were simply and accurately calculated by use of the OCSs, because of the close correlation with the OCSs (gradients = 1.05, $r = 0.97$).

The regression function of the NEC to different patient-dependent parameters showed that the coefficient of determination was higher in the OCS ($R^2 = 0.7178$) than

in the weight and BMI. Based on this fact, the OCS was chosen for patient-dependent parameters. It may be surprising that the coefficients of determination of the weight and BMI have lower values compared with the OCS. Apparently, in our population, the error of weight and BMI in the regression function caused increasing by low-weight and low-BMI. We considered that the injected activity per weight was large for low-weight and low-BMI patients because the injected activity was not adjusted in accordance with the weight. The NEC decreased significantly as the OCS increased, and the relationship between the OCS and the NEC followed an exponential function (Fig. 4c). These findings indicate that the quality of the PET images decreases rapidly as the size of the torso cross-section increases, and that the NEC decreases considerably in overweight patients because the conventional acquisition time of 120 s produces low-quality images. If the cross-section of a patient's torso is extrapolated beforehand, the PET image quality can be improved when the estimated NEC is used. Therefore, we consider that the estimated NEC and OPT could deliver the same image quality if a database of torso cross-sections and the NEC was established. The quality of the images should be roughly maintained by use of an equation based on the OPT. Equation 5 was created for validation of the OPT in a clinical study of the patients from group 3 ($n = 59$). The

average OPT for the underweight patients was slightly shorter (by 13.7 s) (Fig. 5), and the uniformity of the images acquired from these patients was similar to that obtained from conventionally acquired images (Fig. 7). It is possible to shorten the acquisition time for underweight patients, but the uniformity of the PET images may be degraded. Hence, an acquisition time of <120 s was calculated for underweight patient. In contrast, the quality of the images obtained from normal and overweight patients at the conventional acquisition time of 120 s was often poor. The quality of the images obtained from normal and overweight patients improved with use of the OPT, which increased by 14.3 % (137 s), and 43.4 % (172 s), respectively, compared with the conventional acquisition time (Fig. 5). However, the optimized NEC did not improve in overweight patients compared with the standard NEC (Figs. 5, 6). In this regard, we consider that a power function derived from the NEC and OCS presents a problem, because there were few patients with an OCS of $\geq 1300 \text{ cm}^2$ in the study population. Hence, we believe that the power function created was influenced by the median value of OCSs.

A potential limitation associated with this study is that the NECs were calculated from the true, scatter, and random count rates, and from the scatter fraction; therefore, the NEC depends on the injected dose of radiation [12, 13]. The radiation dose for ^{18}F -FDG was fixed at 185 MBq at the time of calibration in this study. Therefore, further studies are needed to confirm our findings with respect to overweight patients and the power function, while the injected dose of radiation is taken into consideration. Furthermore, we propose that the high-accumulation areas, (namely, the heart and kidney) affected the NEC, and that the high-accumulation areas were variable factors associated with the NEC as shown in Fig. 7.

Our findings indicated that optimizing the acquisition time by using a regression function derived from torso cross-sections and the NEC could improve the quality of PET images of the liver, while lower injected doses of radiation are used. The validity of optimizing the PET acquisition time was estimated by calculation of the regression function from torso cross-sections and the NEC.

5 Conclusions

We optimized the quality of PET images to achieve accurate diagnoses. The validity of optimizing the PET acquisition time was estimated by calculation of the regression function from torso cross-sections and the NEC. Our estimates indicated that this acquisition time could be optimized accurately for individual patients. However,

further studies are needed to confirm these findings for overweight patients.

Acknowledgments The authors acknowledge the clinical staff of the Kawasaki Medical School Hospital PET facility for assistance with the clinical data and thank the participants in the Digital Image Scientific Research Meeting in Mihara for helpful discussions.

Compliance with ethical standards

Conflict of interest The authors have no conflict of interest to declare.

References

1. Czernin J, Allen-Auerbach M, Schelbert HR. Improvements in cancer staging with PET/CT: literature-based evidence as of September 2006. *J Nucl Med.* 2007;48(Suppl 1):78S–88S.
2. Swisher SG, Erasmus J, Maish M, Correa AM, Macapinlac H, Ajani JA, et al. 2-Fluoro-2-deoxy-D-glucose positron emission tomography imaging is predictive of pathologic response and survival after preoperative chemoradiation in patients with esophageal carcinoma. *Cancer.* 2004;101:1776–85.
3. Uesaka D, Demura Y, Ishizaki T, Ameshima S, Miyamori I, Sasaki M, et al. Evaluation of dual-time-point ^{18}F -FDG PET for staging in patients with lung cancer. *J Nucl Med.* 2008;49:1606–12.
4. Halpern BS, Dahlbom M, Auerbach MA, Schiepers C, Fueger BJ, Weber WA, et al. Optimizing imaging protocols for overweight and obese patients: a lutetium orthosilicate PET/CT study. *J Nucl Med.* 2005;46:603–7.
5. Watson CC, Casey ME, Bendriem B, Carney JP, Townsend DW, Eberl S, et al. Optimizing injected dose in clinical PET by accurately modeling the counting-rate response functions specific to individual patient scans. *J Nucl Med.* 2005;46:1825–34.
6. De Groot EH, Post N, Boellaard R, Wagenaar NR, Willemsen AT, van Dalen JA. Optimized dose regimen for whole-body FDG-PET imaging. *EJNMMI Res.* 2013;3:63–74.
7. Lartizen C, Comtat C, Kinahan PE, Ferreira N, Bendriem B, Trébossen R. Optimization of injected dose based on noise equivalent count rates for 2- and 3-dimensional whole-body PET. *J Nucl Med.* 2002;43:1268–78.
8. Masuda Y, Kondo C, Matsuo Y, Uetani M, Kusakabe K. Comparison of imaging protocols for ^{18}F -FDG PET/CT in overweight patients: optimizing scan duration versus administered dose. *J Nucl Med.* 2009;50:844–8.
9. Halpern BS, Dahlbom M, Quon A, Schiepers C, Waldherr C, Silverman DH, et al. Impact of patient weight and emission scan duration on PET/CT image quality and lesion detectability. *J Nucl Med.* 2004;45:797–801.
10. Nagaki A, Onoguchi M, Matsutomo N. Patient weight-based acquisition protocols to optimize ^{18}F -FDG PET/CT image quality. *J Nucl Med Technol.* 2011;39:72–6.
11. Mizuta T, Senda M, Okamura T, Kitamura K, Inaoka Y, Takahashi M, et al. NEC density and liver ROI S/N ratio for image quality control of whole-body FDG-PET scans: comparison with visual assessment. *Mol Imaging Biol.* 2009;11:480–6.
12. Macdonald LR, Schmitz RE, Alessio AM, Wollenweber SD, Stearns CW, Ganin A, et al. Measured count-rate performance of the Discovery STE PET/CT scanner in 2D, 3D and partial collimation acquisition modes. *Phys Med Biol.* 2008;53:3723–38.
13. Bettinardi V, Danna M, Savi A, Lecchi M, Castiglioni I, Gilardi MC, et al. Performance evaluation of the new whole-body PET/

- CT scanner: Discovery ST. *Eur J Nucl Med Mol Imaging*. 2004;31:867–81.
14. Shimada N, Daisaki H, Murano T, Terauchi T, Shinohara H, Moriyama N. Optimization of the scan time is based on the physical index in FDG-PET/CT. *Nihon Hoshasen Gijutsu Gakkai Zasshi*. 2011;67:1259–66.
 15. Lodge MA, Mhlanga JC, Cho SY, Wahl RL. Effect of patient arm motion in whole-body PET/CT. *J Nucl Med*. 2011;52:1891–7.
 16. Teräs M, Tolvanen T, Johansson JJ, Williams JJ, Knuuti J. Performance of the new generation of whole-body PET/CT scanners: Discovery STE and Discovery VCT. *Eur J Nucl Med Mol Imaging*. 2007;34:1683–92.
 17. Ollinger JM. Model-based scatter correction for fully 3D PET. *Phys Med Biol*. 1996;41:153–76.
 18. McDermott GM, Chowdhury FU, Scarsbrook AF. Evaluation of noise equivalent count parameters as indicators of adult whole-body FDG-PET image quality. *Ann Nucl Med*. 2013;27:855–61.
 19. Fukukita H, Suzuki K, Matsumoto K, Terauchi T, Daisaki H, Ikari Y, et al. Japanese guideline for the oncology FDG-PET/CT data acquisition protocol: synopsis of version 2.0. *Ann Nucl Med*. 2010;28:693–705.
 20. Chang T, Chang G, Clark JW, Diab RH, Rohren E, Mawlawi OR. Reliability of predicting image signal-to-noise ratio using noise equivalent count rate in PET imaging. *Med Phys*. 2012;39:5891–900.
 21. Chang T, Chang G, Kohlmyer S, Clark JW, Rohren E, Mawlawi OR. Effects of injected dose, BMI and scanner type on NECR and image noise in PET imaging. *Phys Med Biol*. 2011;56:5275–85.
 22. Badawi RD, Marsden PK, Cronin BF, Sutcliffe JL, Maisey MN. Optimization of noise-equivalent count rates in 3D PET. *Phys Med Biol*. 1996;41:1755–76.
 23. El Fakhri G, Santos PA, Badawi RD, Holdsworth CH, Van Den Abbeele AD, Kijewski MF. Impact of acquisition geometry, image processing, and patient size on lesion detection in whole-body ¹⁸F-FDG PET. *J Nucl Med*. 2007;48:1951–60.
 24. Farquhar TH, Llacer J, Sayre J, Tai YC, Hoffman EJ. ROC and LROC analyses of the effects of lesion contrast, size and signal-to-noise ratio on detectability in PET images. *J Nucl Med*. 2000;41:745–54.